Available online at www.sciencedirect.com
ScienceDirect
Trans. Nonferrous Met. Soc. China 31(2021) 1127−1139
Transactions of Nonferrous Metals Society of China
www.tnmsc.cn

Recovery of rare earth element ytterbium(III) by dried powdered biomass of spirulina: Adsorption isotherm, kinetic and thermodynamic study

Qing SHU, Chun-fa LIAO, Wen-qiang ZOU, Bao-quan XU, Yu-hui TAN

Faculty of Materials Metallurgy and Chemistry,
Jiangxi University of Science and Technology, Ganzhou 341000, China

Received 8 April 2020; accepted 26 November 2020

Abstract: The adsorption characteristics and mechanisms of spirulina powder were investigated when it was used as adsorbent to recover ytterbium(III) from wastewater solution. Surface structure and element valence of the adsorbent were analyzed by SEM and XPS for the exploring of its adsorption mechanism for ytterbium(III). The adsorption characteristics of ytterbium(III) on spirulina powder was analyzed through assessing adsorption isotherm, kinetics and thermodynamic models. The adsorption isotherm data were best explained by Langmuir model, and the adsorption capacity of spirulina powder for ytterbium(III) was 72.46 mg/g when adsorption temperature was 318 K. The kinetic experiment results showed that the pseudo-second order kinetic model can better simulate the adsorption process of spirulina powder to ytterbium(III), indicating that the rate-controlling step was chemical adsorption. Spirulina can be an efficient and economical ytterbium(III) recycling material, because it showed good adsorption stability and reusability from the adsorption−desorption cycle experiment results.

Key words: spirulina; ytterbium(III); adsorption; thermodynamics; kinetics

1 Introduction

The recovery of medium and heavy rare earths from rare earth mine wastewater continues to be of high importance since it represents a promising strategy against the global supply crisis of rare earth elements. However, the concentration of rare earth ions in rare earth mine wastewater is usually below 100 mg/L, which makes recovery very difficult. Therefore, it is essential to develop a method for economically and reasonably recovering low-concentration medium and heavy rare earth ions from rare earth wastewater [1,2]. At present, the methods commonly used to treat rare earth waste water include precipitation and ion exchange [3,4]. However, those above two methods are generally costly, less efficient and limited applicability. Also, they will produce a large amount of waste that is noxious or difficult to be decomposed.

As a viable alternative, biological adsorption method has received increasing interest due to their cost-effectiveness and environmental benignity. Also, bio-sorbents are broadly adapted to pH and temperature ranges, and selectively adsorbed low concentration metals [5−11]. The bio-sorption is commonly realized from the passive binding of metal ions with the active functional groups (such as carboxyl groups, hydroxyl groups, amino groups) contained in the polysaccharides, proteins and uronic acids that are rich in the cell walls and some extracelluar products of freshwater algaes. Due to the content and type of active functional groups in the freshwater algae are different, so the different adsorption capacity appeared. Spirulina is a type of filamentous blue-green microalgae (cyanobacteria) that contains high levels of carbonate and bicarbonate, and it is the most abundant in the

Corresponding author: Qing SHU; E-mail: shuqing@jxust.edu.cn
DOI: 10.1016/S1003-6326(21)65566-8

tropical and subtropical lakes. Recently, it has been successfully used as bio-adsorbent for the recovery of Co(II) from leachates of LIB [12].

However, there are few reports on using spirulina to recover rare earth ions. Therefore, the adsorption performance of spirulina for Yb^{3+} was studied, and the possible adsorption mechanism was discussed in this study. It should be noted that when spirulina was used as adsorbent to recover heavy metal ion, the adsorption separation can be achieved through ion exchange. Rare earth ions have a special valence electron configuration, which makes them have a strong electron withdrawing effect. Due to this special property, it is easy to form coordination bonds with some active functional groups, such as amino groups, and it is achieved by the way that the nitrogen atoms on $—NH_2$ provides a pair of lone electrons. Therefore, when spirulina is used as adsorbent to recover rare earth ions, the recovery may be mainly realized from the formation of coordination bonds. As the cell wall of dry spirulina power is broken, which can expose more cell surface functional groups, so the adsorption efficiency of the dried spirulina is often higher than that of live algae. Therefore, dry spirulina powder was chosen as bio-adsorbent in this study. Moreover, the influences of various parameters on the adsorption efficiency of spirulina powder have been studied, such as contact time, spirulina powder dosage and pH. Adsorption equilibrium, kinetics, and thermodynamic parameter were evaluated to understand the nature of this adsorption process.

2 Experimental

2.1 Culture of bio-adsorbent

The culture processes of spirulina are as follows: (1) the algae species were placed in Zarrouk medium and exposed continuous illumination through a cold light source 3000 lx with rotation (90 r/min) at 298 K for 24 h; (2) the spirulina was subsequently separated from the culture medium by centrifugation at 8000 r/min (8 min); (3) the supernatant was discarded, and the precipitate was washed five times with distilled water; (4) the precipitate was dried in an oven at 343 K for 24 h; (5) the dried spirulina was ground to a fine powder (<250 μm) and sieved through a 75−100 μm sieve, and which was used for all further processes.

2.2 Bio-adsorbent characterization

A MLA650 scanning electron microscopy (SEM, FEI, USA) was used to investigate the surface morphology of the spirulina before and after adsorption of Yb^{3+}. The bond type of the spirulina before and after adsorption of Yb^{3+} were analyzed by the multifunctional imaging electron energy spectrometer XPS (Thermo Scientific Escalab 250Xi, Thermo Scientific, USA) using a monochromatic Al K_α ($h\nu$=1486.6 eV) with 150 W power and 500 μm beam spot.

2.3 Batch adsorption studies

A stock solution of Yb^{3+} (1000 mg/L) was prepared in distilled water using an accurate quantity of $Yb(NO_3)_3$ (99.9%, AR, Aladdin Reagent Co., Ltd.). Yb^{3+} solutions at other concentrations were prepared from the stock solution by dilution and varied from 50 to 300 (mg/L). To determine the optimum pH, contact time and spirulina powder dosage and initial concentration for the adsorption process, batch adsorption experiments were performed at 298−318 K. The initial pH values of the Yb^{3+} solutions were adjusted from 2.0 to 6.0 using 1 mol/L H_2SO_4 or 1 mol/L NaOH, 0.1−0.8 g of spirulina was added into 100 mL of Yb^{3+} solution (100 mg/L), and contact time was varied from 10 to 150 min. The samples were analyzed to determine the Yb^{3+} concentration by using Inductively Coupled Plasma-Atomic Emission Spectrometry (ICP-AES, GB/T 18115.11 — 2006). After the adsorption test, the adsorbent and adsorbate were separated by centrifugation.

The adsorption efficiency (A) of Yb^{3+} on the spirulina biosorbent was calculated by

$$A=\frac{C_0-C_e}{C_0}\times 100\% \quad (1)$$

where C_0 and C_e (mg/L) represent the initial and equilibrium concentrations of Yb^{3+} in the solution, respectively.

2.4 Desorption experiment

Various desorption agents such as 0.1 mol/L ethylendiamine tetraacetic acid (EDTA), 0.1 mol/L HCl and 0.1 mol/L HNO_3 were used in this study. For desorption study, the spirulina was recovered from the Yb^{3+} solution using a filter after the

adsorption experiments. The spirulina was washed with distilled water under agitation at 180 r/min for 10 min for the removing of the residual Yb^{3+} on its surface, and this washing process was repeated three times. The spirulina was then soaked in 100 mL of desorption agent, and the mixtures were shaken overnight. The relative desorption efficiency (D) was calculated as

$$D=\frac{C_d}{C_a}\times 100\% \quad (2)$$

where C_d is the desorbed amount of Yb^{3+} by desorption agent, and C_a is the adsorbed amount of Yb^{3+} by spirulina powder.

2.5 Adsorption isotherm models

In this study, four models (Langmuir, Freundlich, Redlich−Peterson and Dubinin−Radushkevich) were applied to study the adsorption isotherm of Yb^{3+} by spirulina. And the prediction accuracy of these above four models has been compared to determine which one is the best fit model.

Langmuir model was used for modeling the adsorption of Yb^{3+} on homogeneous surfaces without any interaction between the adsorbed ions. The Langmuir isotherm can be explained by [13]:

$$q_{eq}=\frac{q_m K_L C_e}{1+K_L C_e} \quad (3)$$

where q_{eq} (mg/g) is the amount of Yb^{3+} on the adsorbent at equilibrium, q_m (mg/g) is the monolayer bio-sorption capacity of the adsorbent, and K_L (L/mg) is the Langmuir adsorption constant, which is related to the free energy of adsorption.

The essential features of the Langmuir isotherm can be expressed in terms of equilibrium parameter R_L, which is a dimensionless constant referred to as the separation factor or equilibrium parameter. It can be defined by

$$R_L=\frac{1}{1+K_L C_0} \quad (4)$$

In contrast, the Freundlich model describes the adsorption of metal ions on the heterogeneous surfaces. It can be defined by [14]

$$q_{eq}=K_F C_e^{1/n_F} \quad (5)$$

where K_F is a constant related to the adsorption capacity, and $1/n_F$ is an empirical parameter related to the adsorption intensity, which varies with the heterogeneity of the material.

The Redlich−Peterson isotherm contains three parameters and incorporates the features of the Langmuir and the Freundlich isotherms. It can be described as [15]

$$\ln\left(K_{R\text{-}P}\frac{C_e}{q_{eq}}-1\right)=g\ln C_e+\ln a_{R\text{-}P} \quad (6)$$

where $a_{R\text{-}P}$ (L/mg) and $K_{R\text{-}P}$ (L/mg) are Redlich–Peterson isotherm constants, and g (mol^2/kJ^2) is the activity coefficient of adsorption energy.

The Dubinin−Radushkevich model is generally applied to expressing the adsorption mechanism with a Gaussian energy distribution on the heterogeneous surface. It can be described as the following equations [16]:

$$q_{eq}=q_s\exp(-\beta\varepsilon^2) \quad (7)$$

$$\varepsilon=RT\ln[1+(1/C_e)] \quad (8)$$

$$E=\frac{1}{(2\beta)^{1/2}} \quad (9)$$

where q_s (mg/L) is the theoretical isotherm saturation adsorption capacity, β (mol^2/kJ^2) is the activity coefficient of adsorption energy, ε is the Dubinin-Radushkevich isotherm constant, and E (kJ/mol) is the mean adsorption free energy.

2.6 Thermodynamics of adsorption

A series of adsorption experiments were conducted at 298−318 K to study the thermodynamics of adsorption of Yb^{3+} on spirulina. Adsorption experimental conditions are as follows: pH of the solution was 5, the contact time was 60 min, the adsorbent dosage was 2 g/L, and the initial Yb^{3+} concentrations ranged from 100 to 300 mg/L. The changes in thermodynamic parameters such as the Gibbs free energy (ΔG^Θ), enthalpy (ΔH^Θ) and entropy (ΔS^Θ) for the Yb^{3+} adsorption process are obtained by using the following equations:

$$\Delta G^\Theta=-RT\ln K_T \quad (10)$$

$$K_T=55.5\times 1000\times 173.04K_L \quad (11)$$

$$\ln K_T=\frac{\Delta S^\Theta}{R}-\frac{\Delta H^\Theta}{RT} \quad (12)$$

where K_T is the dimensionless parameter calculated from Eq. (11) using K_L, 55.5 is the number of moles

of pure water per litre, 173.04 g/mol is the molar mass of Yb (solute), R is the gas constant (8.314 J/(mol·K)), and T is temperature (K). The conversion of K_L to K_T is strongly recommended for correct thermodynamic parameters calculation [17].

2.7 Kinetic experiments

The experimental data used in the kinetic study are the same as those used in the thermodynamic study. Adsorption kinetic models, such as pseudo-first order, pseudo-second order, Elovich kinetic and intra-particle diffusion, were used to interpret the experimental data for understanding the adsorption kinetics of Yb^{3+} on spirulina powder. And the prediction accuracy of those above kinetic models has been compared in order to determine which one is the best fit model.

The equation used for the pseudo-first order kinetic model is expressed as [18]

$$\ln(q_{eq}-q_t)=\ln q_{eq}-k_1 t \tag{13}$$

where q_t (mg/g) is the adsorption capacity at time t, and k_1 (min^{-1}) is the rate constant of the pseudo-first order adsorption.

The equation used for the pseudo-second order kinetic model is expressed as [19,20]

$$\frac{t}{q_t}=\left(\frac{1}{k_2 q_{eq}^2}\right)+\left(\frac{1}{q_{eq}}\right)t \tag{14}$$

where k_2 (g/(mg·min)) is the rate constant of the pseudo-second order adsorption. The linear form of elovich kinetic model is expressed as

$$q_t=\frac{1}{b}\ln(ab)+\frac{1}{b}(\ln t) \tag{15}$$

where a (mg/(g·min)) is the initial adsorption rate, and b (g/mg) is the Elovich desorption constant.

The linear form of the intra-particle diffusion models is expressed as [21]

$$q_t=k_p t^{1/2}+C \tag{16}$$

where k_p (mg/(g·$min^{1/2}$)) is the rate constant of the intra-particle diffusion, and C (mg/g) gives an idea about the thickness of the boundary layer.

3 Results and discussion

3.1 Characterization of spirulina powder

SEM images of the spirulina before and after adsorption of Yb^{3+} are shown in Fig. 1. It can be seen from Fig.1 that the morphological structure of spirulina has been significantly changed after adsorption of Yb^{3+}, and the surface of spirulina was squeezed into wrinkles. The change of the morphology structure indicated a good accessibility of Yb^{3+} onto the surface of spirulina.

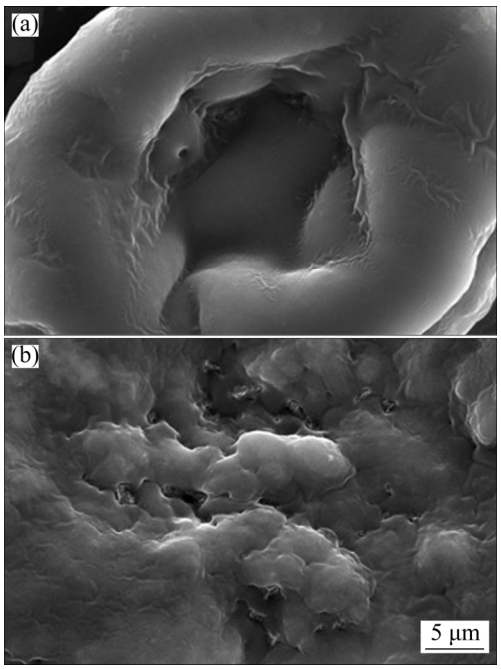

Fig. 1 SEM images of spirulina before (a) and after (b) adsorption of Yb^{3+}

In order to investigate the change in the chemical valences of the surface functional group on the spirulina before and after adsorption of Yb^{3+}, they were further characterized by the XPS test, and the results are shown in Fig. 2.

Figure 2(a) shows that the N1s pattern and two binding energy peaks appeared at 399.73 and 400.40 eV, which can be assigned to the C—NH_2 band [22,23]. And the binding energy peaks were slightly shifted towards high energy (399.93 and 400.62 eV) after adsorption of Yb^{3+}. Figure 2(b) shows the Yb 4d pattern, two binding energy peaks appeared at the 185.4 and 190.8 eV, which respectively corresponded to the Yb $4d_{5/2}$ and Yb $4d_{3/2}$ [24]. Based on these above XPS results, it can be inferred that the interaction occurred between nitrogen and Yb atoms. ÇELEKLI et al [25] and LARROSA et al [26] once mentioned that the spirulina contains several functional groups, such as amine, carboxyl, hydroxyl, aldehyde, ketone, phosphate and sulfate, which are capable to interact with the ions in solution. It can be speculated that a

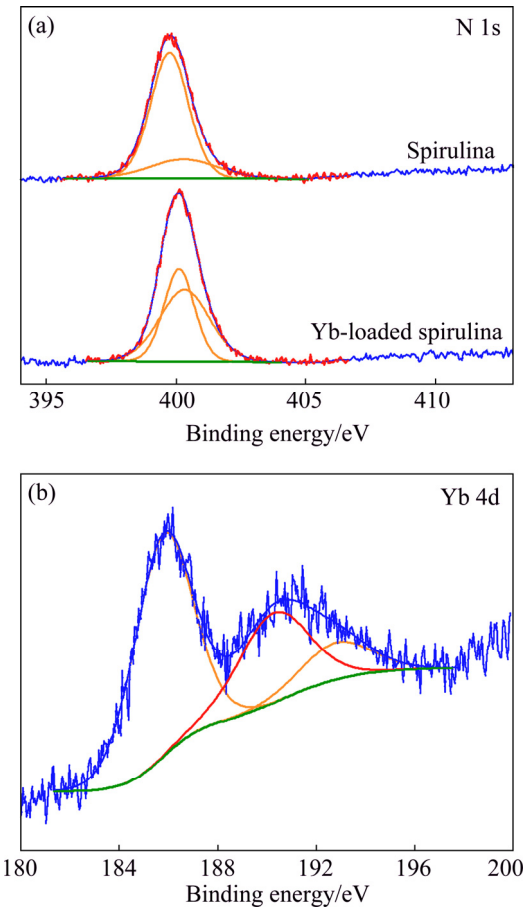

Fig. 2 X-ray photoelectron spectra of spirulina before and after adsorption of Yb^{3+}: (a) N1s; (b) Yb 4d

coordinate bond has formed through the electron sharing between the amino group of spirulina and Yb^{3+}. The possible reasons are as follows: due to the strong electric induction effect exerted by Yb^{3+}, the shielding effect of the outer layer electrons on the core layer electrons of N element is reduced, so the valence electron layer density of N element was reduced. It directly affects the electronic state of N and Yb^{3+} and increases the imbalance of the system. Hence, the binding energy of the core electrons of the N element was increased. As a result, a lone pair of electron of (═N—) would donate to Yb^{3+} and form nitrogen atom of doped imine (═N^{+}—). Thus, the adsorption capacity of spirulina to Yb^{3+} was improved. Taking into account the element and chemical valences analytical results, it is reasonable to speculate that the adsorption is closely related to the amine group of spirulina.

3.2 Effect of adsorption conditions

The pH of the solution is one of the most important factors that greatly affect the metal ion adsorption process because the adsorption efficiency is closely related to the charge of the metal ions and the metal-binding site of the adsorbent. And both of them can be influenced by pH of the solution. To obtain the best pH for Yb^{3+} adsorption, the effect of pH on the Yb^{3+} adsorption by spirulina was investigated in the range of 2.0−6.0. Other adsorption experimental conditions were as follows: contact time was 60 min, adsorption temperature was 298 K and adsorbent dosage was 1 g/L, initial Yb^{3+} concentrations were 50 and 100 mg/L. The effect of pH on the adsorption efficiency of Yb^{3+} is shown in Fig. 3.

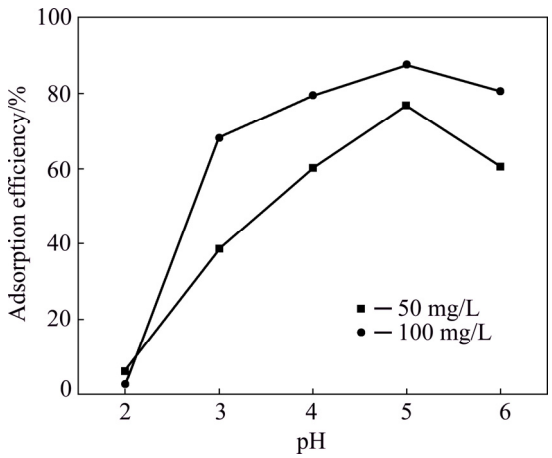

Fig. 3 Effect of pH on adsorption efficiency (contact time 60 min, adsorption temperature 298 K, adsorbent dosage 1 g/L, and initial Yb^{3+} concentrations 50 and 100 mg/L)

Figure 3 shows that the adsorption of Yb^{3+} onto spirulina increases with the increase of solution pH when the pH is less than 6.0. The maximum adsorption efficiency was 87.62% when the pH was 5.0 and the initial concentration of Yb^{3+} was 100 mg/L. The adsorption efficiency begins to decrease when the pH increases to 6.0. The pH value of the adsorption solution not only affects the electronegativity of the surface groups of the adsorbent, but also affects the binding capacity of hydrogen ions and metal ions [27]. When the pH of the solution is lower than a certain level, the functional groups on the surface of the spirulina cell wall are protonated and the adsorbent is positively charged. The electrostatic repulsion generated at this time affects the ability of the adsorbent to adsorb Yb^{3+}. The lower the pH is, the greater the repulsion becomes. The lower the pH of the solution is, the greater the density of positively

charged groups on the surface of the adsorbent becomes, and the greater the electrostatic mutual repulsion effect between Yb^{3+} and positively charged groups. When the pH value gradually increases, more reactive groups will be negatively charged, thereby providing more adsorption sites, and positively charged Yb^{3+} occupies the adsorption sites on the surface, of the spirulina cell wall so the ability to absorb Yb^{3+} increases. Too high pH also has an adverse effect on metal adsorption. When the pH of the solution exceeds the metal ion solubility product constant, a large amount of metal ions in the solution will generate oxide precipitation, making the adsorption process impossible. Therefore, the pH was fixed at 5.0 for further batch experiments.

Adsorbent dosage can determine the adsorption capacity of an adsorbent for a given initial concentration of the adsorbate in the liquid phase, so it is important to investigate the effect of adsorbent dosage on the adsorption capacity. The effect of adsorbent dosage on the Yb^{3+} recovery was investigated in the range from 0.4 to 8 g/L. Other adsorption experiment parameters were carried out as follows: contact time was 60 min, pH was 5.0 and adsorption temperature was 298 K, initial Yb^{3+} concentration was 100 mg/L. The effect of spirulina dosage on the adsorption efficiency of Yb^{3+} is shown in Fig. 4.

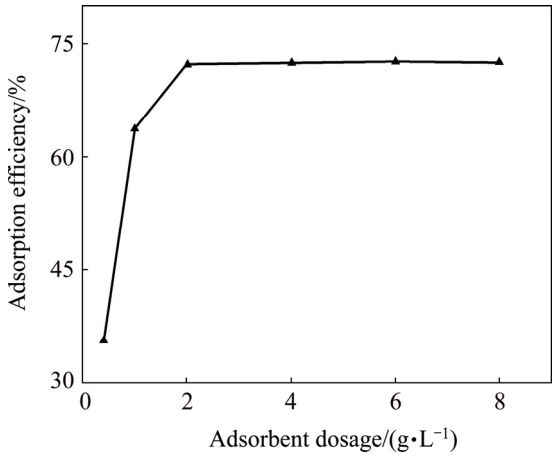

Fig. 4 Effect of spirulina dosage on adsorption efficiency (contact time 60 min, pH 5.0, adsorption temperature 298 K, and initial Yb^{3+} concentration 100 mg/L)

Figure 4 shows that the adsorption of Yb^{3+} onto spirulina increases with the increase of spirulina dosage when the dosage is less than 6. The adsorption efficiency begins to decrease when the dosage of spirulina increases to 4 g/L. This result indicated that the spirulina dosage of 2.0 g/L was effective in complete adsorption of 50 mg/L Yb^{3+}. Therefore, this biosorbent dosage was fixed for at 2.0 g/L further batch experiments.

Effect of contact time on the Yb^{3+} recovery by the spirulina was investigated in the range from 10 to 150 min. Other adsorption experimental conditions were as follows: pH was 5.0, the adsorption temperature was 298 K, initial Yb^{3+} concentrations were in the range from 100 mg/L to 300 mg/L. The effect of contact time on the adsorption efficiency of Yb^{3+} is shown in Fig. 5. It shows that the adsorption efficiency of the Yb^{3+} increased instantly at the initial 30 min and continued to increase gradually until the equilibrium was reached at 60 min. Therefore, contact time of 60 min was fixed for further batch experiments.

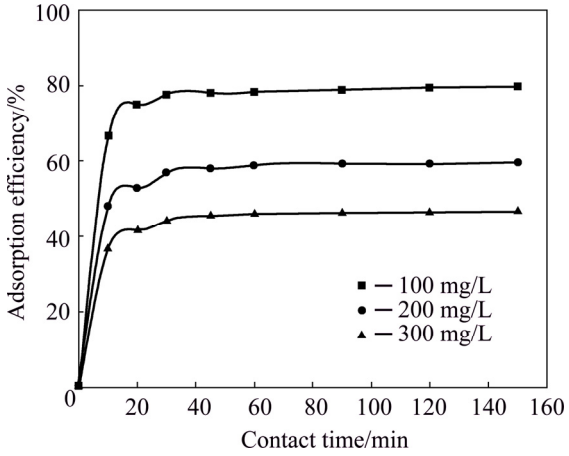

Fig. 5 Effect of contact time on adsorption efficiency (pH 5.0, adsorption temperature 298 K, adsorbent dosage 2 g/L, and initial concentration of Yb^{3+} 100−300 mg/L)

3.3 Adsorption isotherms

The adsorption isotherm can provide information about the distribution of adsorption molecules between the liquid phase and solid phase at an equilibrium state. A suitable adsorption isotherm model can be found based on the fitting of isotherm data to various isotherm models. The specific relationship between the concentration of Yb^{3+} and its degree of accumulation onto the surface of spirulina was explained by the adsorption isotherm study. In this study, the different isotherm models such as Langmuir, Freundlich, Redlich−Peterson (R−P) and Dubinin−Radushkevich (D−R) were employed for fitting the experimental

equilibrium adsorption data. Results are shown in Fig. 6.

Non-linear regression analysis of adsorption isotherm (Fig. 6) was carried out to determine the adsorption parameters and the non-linear regression coefficients. The obtained adsorption isotherm parameters along with the non-linear regression coefficients are shown in Tables 1−3.

It can be seen from Table 1 that the R^2 was range from 0.99−1.00 in the Langmuir model and 0.71−0.96 in the Freundlich model. The R^2 was ranged from 0.92−0.96 in the Redlich−Peterson (R−P) model (Table 2) and 0.93−1.00 in the Dubinin−Radushkevich (D−R) model (Table 3). These values were sufficiently high suggesting that the Langmuir, Redlich−Peterson and Dubinin−Radushkevich are able to describe the biosorption of Yb^{3+} well. However, it can be concluded that the Langmuir model was a more appropriate model than Freundlich, Redlich−Peterson and Dubinin−Radushkevich models when R^2 values were compared.

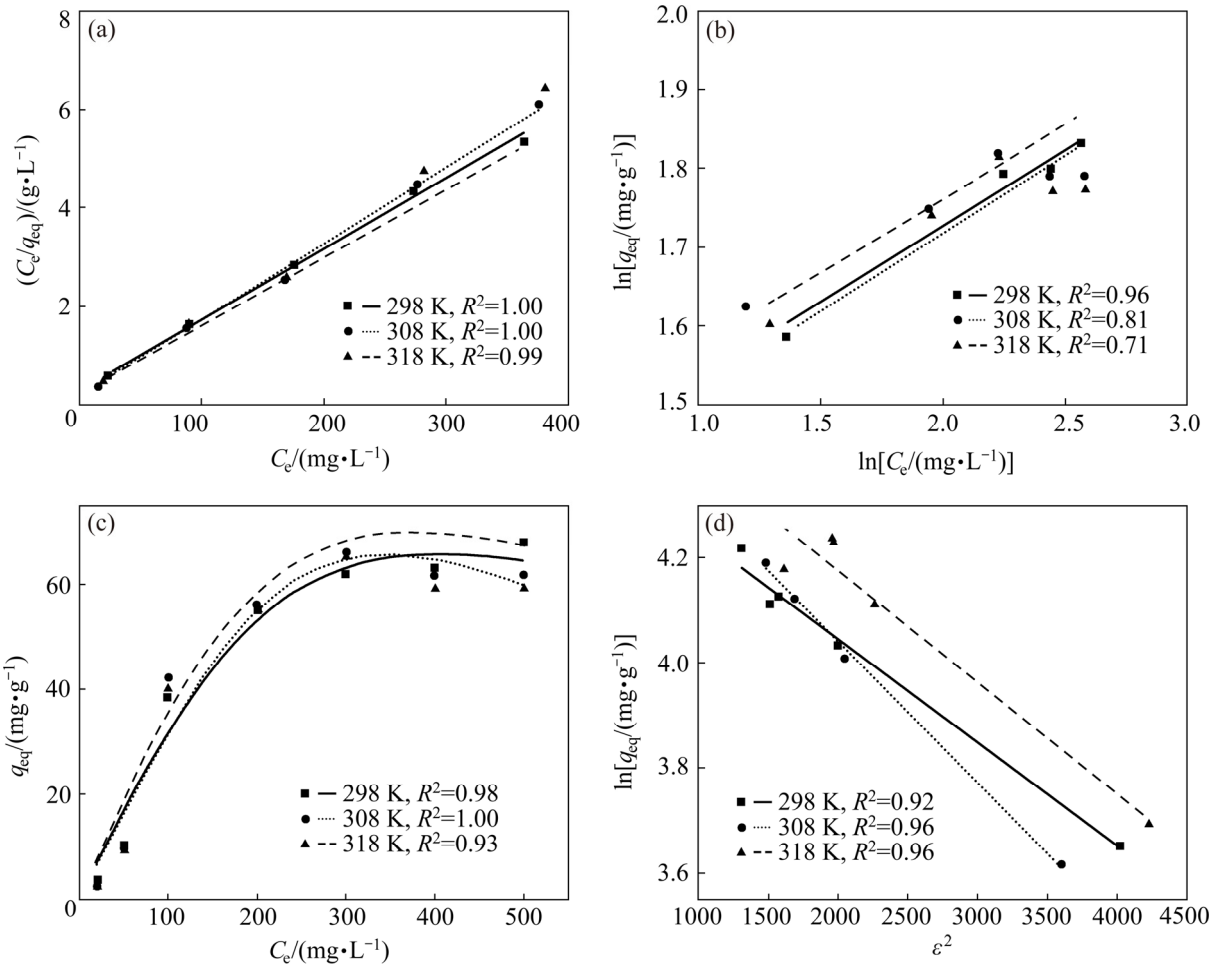

Fig. 6 Adsorption isotherm: (a) Langmuir isothermal adsorption model; (b) Freundlich isothermal adsorption model; (c) Redlich−Peterson model; (d) Dubinin−Radushkevich model

Table 1 Adsorption parameters and non-linear regression coefficients (Langmuir and Freundlich models)

T/K	Langmuir			Freundlich		
	$q_m/(mg\cdot g^{-1})$	$K_L/(L\cdot g^{-1})$	R^2	$K_F/(L\cdot g^{-1})$	n_F	R^2
298	64.94	0.05	1.00	22.06	5.20	0.96
308	69.93	0.08	1.00	21.14	5.08	0.81
318	72.46	0.06	0.99	24.41	5.34	0.71

Table 2 Adsorption parameters and non-linear regression coefficients (Redlich−Peterson model)

T/K	$K_{R\text{-}P}$/ ($L\cdot g^{-1}$)	$a_{R\text{-}P}$/ (10^{-4} $L\cdot g^{-1}$))	g/ ($mol^2\cdot kJ^{-2}$)	R^2
298	0.34	1.23	1.90	0.92
308	0.33	1.24	2.33	0.96
318	0.39	1.23	1.92	0.96

Table 3 Adsorption parameters and non-linear regression coefficients (Dubinin−Radushkevich model)

T/K	β/($10^{-4}mol^2\cdot kJ^{-2}$))	E/($kJ\cdot mol^{-1}$)	R^2
298	1.97	15.93	0.98
308	2.68	13.66	1.00
318	2.12	15.36	0.93

The monolayer adsorption capacity (q_m) calculated from the Langmuir model was in the range of 64.94−72.46 mg/g within a temperature range of 298−318 K. It suggested an endothermic nature of Yb^{3+} adsorption on spirulina because adsorption capacity appeared to increase with an increase in the temperature (Table 1). The R_L value calculated from Eq. (4) was in the range of 0.04−0.18 within an initial concentration of Yb^{3+} ranging from 100 to 300 mg/L. This parameter value ($0<R_L<1$) indicated that the spirulina was a suitable adsorbent for the adsorption of Yb^{3+} from aqueous solution. From the linear plot of Freundlich isotherm, K_F and n were calculated as 22.06 L/g and 5.20 respectively. The adsorption process is found to be favorable adsorption when $1/n_F$ value lies between 0 and 1, whereas $1/n_F>1$, and $1/n_F=0$ or 1 indicate unfavorable, and irreversible or linear adsorption respectively. Therefore, the adsorption of Yb^{3+} onto spirulina was favorable under the studied experimental conditions.

The value of g calculated from R−P isotherm model can be used to test the suitability of Langmuir model for the adsorption of Yb^{3+} on spirulina, and it was in the range of 1.900−2.330 within a temperature range of 298−318 K. Therefore, it can be stated that the adsorption of Yb^{3+} onto spirulina can be well explained by the Langmuir model, and this adsorption process is related to a saturated monolayer of adsorbate molecules on the adsorbent surface [12]. The D−R isotherm model can be used to distinguish the adsorption of Yb^{3+} onto spirulina between the physical process and chemical process. The mean adsorption energy E can judge adsorption mechanism as chemical ion exchange or physical adsorption. If E value is in the range of 8−16 kJ/mol, it indicates that the adsorption process is controlled by chemical adsorption mechanism; if E value is less than 8 kJ/mol, it indicates that the adsorption is a physical process [11]. It can be found from Table 3 that the E value of the adsorption of Yb^{3+} onto spirulina powder was in the range of 13.66−15.93 kJ/mol within a temperature range of 298−318 K, indicating that this adsorption process is controlled by chemical adsorption mechanism.

3.4 Thermodynamic evaluation process

The ΔH^Θ and ΔS^Θ values were calculated from the slope and intercept of a linear plot of ln K_T vs $1/T$. The values of all thermodynamic parameters (ΔG^Θ, ΔH^Θ and ΔS^Θ) are listed in Table 4. The ΔG^Θ was found to be −3.09, −3.20 and −3.32 kJ/mol for the adsorption of Yb^{3+} onto spirulina powder at 298, 308 and 318 K respectively. The negative ΔG values indicated that the adsorption of Yb^{3+} onto spirulina powder was feasible and spontaneously thermodynamical. The ΔH^Θ parameter had a value of 0.41 (kJ/mol). The positive ΔH^Θ value indicated the endothermic nature of the adsorption. The ΔS^Θ parameter was found to be 11.72 J/(mol·K). The positive value of ΔS^Θ suggested an increase in the randomness at solid/solution interface during the adsorption of Yb^{3+} onto spirulina powder.

Table 4 Thermodynamic parameters of spirulina after adsorption of Yb^{3+}

T/K	ΔG^Θ/ ($kJ\cdot mol^{-1}$)	ΔS^Θ/ ($J\cdot mol^{-1}\cdot K^{-1}$)	ΔH^Θ/ ($kJ\cdot mol^{-1}$)
298	−3.09		
308	−3.20	11.72	0.41
318	−3.32		

3.5 Adsorption kinetics of ytterbium ions

Adsorption kinetics studies can reveal the mechanism of adsorption and potential rate-controlling steps such as mass transport or chemical reaction processes, so they are useful to find the optimum experimental conditions for full-scale adsorption process. In this study, the different

kinetic models such as the pseudo first-order and pseudo second-order, Elovich and intraparticle diffusion models were employed to study the adsorption of Yb^{3+} on spirulina. The results are shown in Fig. 7. Using those above adsorption kinetics, the amount of Yb^{3+} adsorbed on spirulina powder was calculated. The obtained adsorption kinetic parameters along with R^2 are shown in Tables 5 and 6.

It can be seen from Table 5 that the R^2 was 0.99−1.00 in the pseudo first-order adsorption kinetic model and 1.00 in the pseudo second-order adsorption kinetic model. The R^2 ranged from 0.72−0.82 in the Elovich adsorption kinetic model and 0.53−0.63 in the intraparticle diffusion adsorption kinetic model (Table 6). It can be concluded that the pseudo-second order kinetic model was a more appropriate model than pseudo first-order, Elovich and intraparticle diffusion models when the R^2 values were compared. The obtained values of R^2 being low indicates the Elovich and intraparticle diffusion kinetic models were not agreed with the experimental adsorption data and the recovery of Yb^{3+} from aqueous solution

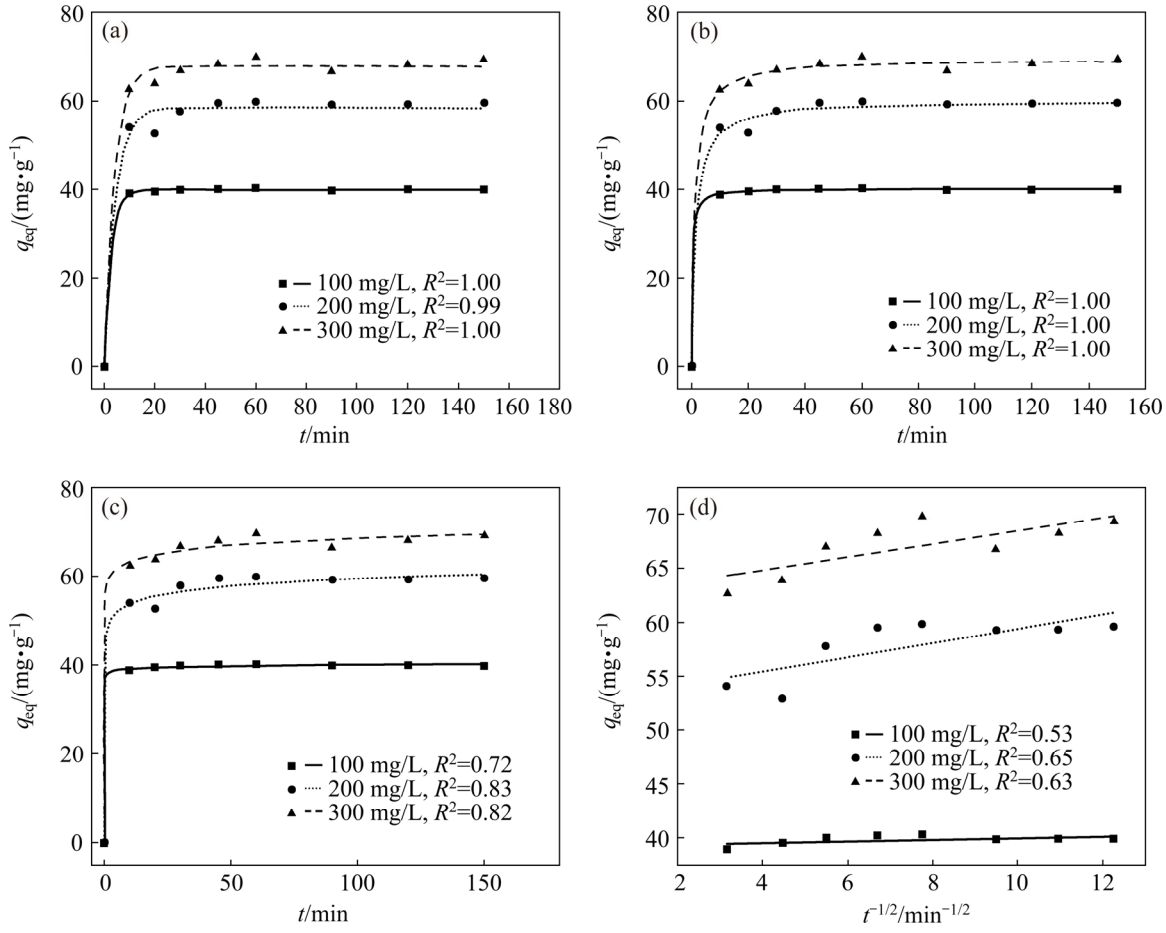

Fig. 7 Kinetic results of Yb^{3+} adsorption on spirulina biosorbent: (a) Pseudo-first-order equation; (b) Pseudo-second-order dynamic equation; (c) Elovich equation; (d) Intra-particle diffusion model

Table 5 Comparison of pseudo first-order and pseudo second-order adsorption kinetic model parameters obtained at different initial Yb^{3+} concentrations for adsorption on spirulina biosorbent at 298 K

C_0/(mg·L^{-1})	Pseudo first-order			Pseudo second-order		
	q_{eq}/(mg·g^{-1})	k_1/min^{-1}	R^2	q_{eq}/(mg·g^{-1})	k_2/(g·mg^{-1}·min^{-1})	R^2
100	39.39	0.18	1.00	40.74	0.012	1.00
200	58.54	0.16	0.99	61.24	0.006	1.00
300	68.67	0.15	1.00	72.01	0.005	1.00

Table 6 Comparison of Elovich and intra-particle diffusion adsorption kinetic model parameters obtained at different initial Yb^{3+} concentrations for adsorption on spirulina biosorbent at 298 K

C_0/(mg·L^{-1})	Elovich			Intra-particle diffusion		
	a/(mg·g^{-1}·min^{-1})	b/(g·mg^{-1})	R^2	C/(mg·g^{-1})	k_p/(mg·g^{-1}·min$^{-1/2}$)	R^2
100	30.51	0.49	0.72	34.45	0.53	0.53
200	40.73	0.24	0.83	48.49	1.09	0.65
300	46.43	0.20	0.82	56.12	1.35	0.63

onto the surface of the spirulina cannot be explained using these two kinetic models. Although the fitting correlation of the internal diffusion kinetic model is not very good, it can be used to study the adsorption mechanism. Generally, if plots of q_t versus $t^{1/2}$ pass through the origin, pore diffusion is the only rate limiting step; if not, it is considered that the adsorption process is also controlled by film diffusion in some cases [21]. It can be seen from Fig. 7 that the plots of q_t versus $t^{1/2}$ did not pass through the origin. Hence, intraparticle diffusion is not the only rate limiting mechanism. In the light of these results, it can speculate that the adsorption of Yb^{3+} onto spirulina is a complex process and both intraparticle diffusion and surface sorption contribute to the rate-limiting step.

3.6 Desorption performance

In order to apply spirulina powder to treating real wastewater, the desorption process of Yb^{3+} is very important. Hence, EDTA (0.05, 0.1 mol/L), HCl (0.05, 0.1 mol/L), and HNO_3 (0.05, 0.1 mol/L) were used for desorption of Yb^{3+} from spirulina. The temperature of desorption is 318 K and the desorption time is 5 min. The results are shown in Fig. 8.

As shown in Fig. 8, desorption ratio of Yb^{3+} using 0.1 mol/L HNO_3 can reach up to 92.3%, which is higher than other desorbents. Table 7 shows the adsorption capacity at equilibrium for different types of rare earth metal ions over different adsorbents collected from the literature.

The obtained adsorption capacity value from this study is higher than most adsorbents listed in Table 7. In addition, the adsorption rate of Yb^{3+} can be maintained at 71.4% after being recycled five times, so the recyclability is acceptable. Hence, spirulina powder could be a green alternative for Yb^{3+} recovery, because it showed good adsorption performance to it.

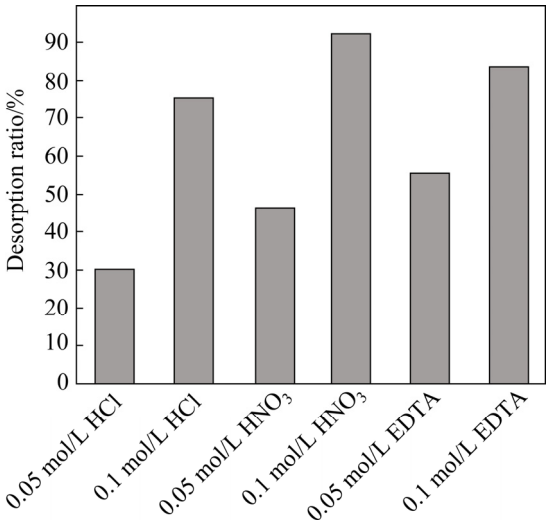

Fig. 8 Desorption ratio of Yb^{3+} for various desorbents (desorption temperature 318 K, and desorption time 5 min)

Table 7 Comparison of adsorption capacity of spirulina with other adsorbents to remove rare earth ions

Adsorbent	Rare earth ions	Adsorption capacity/ (mg·g^{-1})	Ref.
Spirulina	Yb^{3+}	87.6	This study
ZIF-8	La^{3+}	385.0	[28]
MIL-101	La^{3+}	14.6	[29]
MIL-101-DETA	La^{3+}	39.7	[29]
MIL-101-PMIDA	La^{3+}	37.2	[29]
Magnetite@MIL-101-SO3	Ce^{3+}	34.8	[30]
MOF-808-EDTA	La^{3+}	200.0	[31]

3.7 Adsorption difference with coexisting of other rare earth metal ions

Rare earth mine wastewater is usually a complex system containing multiple rare earth ions. At this time, the multiple rare earth ions in the wastewater will generate competitive adsorption site, interfere with the adsorption process of target ions, thereby affecting the adsorption capacity of

the target rare earth ion on biosorbent. For this reason, the adsorption experiments of the difference in the adsorption effect of spirulina powder to Yb^{3+} was carried out when other rare earth metal ions coexist. Three sets of mixed solutions were respectively configured (100 mg/L Er^{3+}+100 mg/L Yb^{3+}; 100 mg/L Pr^{3+}+100 mg/L Yb^{3+}; 100 mg/L Er^{3+}+100 mg/L Pr^{3+}+100 mg/L Yb^{3+}. The result is shown in Fig. 8. It can be seen from Fig. 8 the mixing of multiple rare earth ions will cause the adsorption capacity of spirulina powder to Yb^{3+} decrease. The possible reasons are as follows: the covalent indexes of different rare earth ions are similar. Therefore different rate earth metal ions are easy to form coordination bonds with the amino groups on the cell wall of spirulina powder, thereby forming a competitive adsorption, resulting in a decrease in its adsorption capacity for Yb^{3+}.

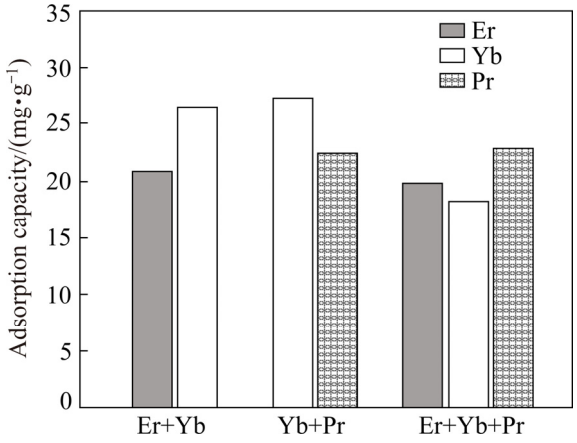

Fig. 8 Adsorption effect of spirulina on Yb^{3+} when other rare earth metal ions coexisting

4 Conclusions

(1) The highest adsorption rate and desorption rate reached 87.6% and 92.3%, respectively.

(2) The high adsorption capacity of spirulina to Yb^{3+} was derived from the formation of coordination bridging between Yb^{3+} and —NH_2 of spirulina powder.

(3) Through the Langmuir isotherm analysis, spirulina showed the maximum Yb^{3+} adsorption capacity of 72.46 mg/g.

(4) Kinetic studies indicated the experimental data were fitted well by the pseudo-second-order model, and the rate-controlling step was chemical adsorption.

(5) The adsorption of Yb^{3+} onto spirulina powder was an endothermic and spontaneous process at the temperatures under investigation (298−318 K).

Acknowledgments

The authors are grateful for the financial supports from the National Natural Science Foundation of China (21766009, 21761013), and the Program of Qingjiang Excellent Young Talents for the Jiangxi University of Science and Technology, China.

References

[1] ZHOU Q, FU Y X, ZHANG X, LUO T T, LUO W J. Light induced growth of polyelectrolyte brushes on kaolinite surface with superior performance for capturing valuable rare-earth Ce^{3+} from wastewater [J]. Materials Science and Engineering B, 2018, 227: 89−99.

[2] FENG Y F, SUN H J, HAN L F, XUE L H, CHEN Y D, YANG L Z, XING B S. Fabrication of hydrochar based on food waste (FWHTC) and its application in aqueous solution rare earth ions adsorptive removal: Process, mechanisms and disposal methodology [J]. Journal of Cleaner Production, 2019, 212: 1423−1433.

[3] ZHANG K, KLEIT N A, NIETO A. An economics strategy for criticality—Application to rare earth element yttrium in new lighting technology and its sustainable availability [J]. Renewable and Sustainable Energy Reviews, 2017, 77: 899−915.

[4] PARK D M, REED D W, YUNG M C, ESLAMIMANESH A, LENCKA M M, ANDERKO A, FUJITA Y, RIMAN R E, NAVROTSKY A, JIAO Y Q. Bioadsorption of rare earth elements through cell surface display of lanthanide binding tags [J]. Environmental Science & Technology, 2016, 50: 2735−2742.

[5] GAO S, LUO T T, ZHOU Q, LUO W J. A novel and efficient method on the recovery of nanosized CeO_2 in Ce^{3+} wastewater remediation using modified sawdust as adsorbent [J]. Journal of Colloid & Interface Science, 2018, 512: 629−637.

[6] CHEN J D, LUO W J, GUO A F, LUO T T, LIN C, LI H F, JING L R. Preparation of a novel carboxylate-rich palygorskite as an adsorbent for Ce^{3+} from aqueous solution [J]. Journal of Colloid & Interface Science, 2018, 512: 657−664.

[7] LI Y, FAN S S, ZHOU Q. Synthesis of carboxyl-rich biosorbent by UV-induced graft polymerization method for high efficiency adsorption of Ce^{3+} from aqueous solution: Activation and adsorption mechanism [J]. Journal of Polymers and the Environment, 2019, 27: 2259−2266.

[8] NOURBAKHSH M, ÖZER Y S D, AKSU Z, KUTSAL T, ÇAğLARA A. A comparative study of various biosorbents for removal of chromium (VI) ions from industrial waste waters [J]. Process Biochemistry, 1994, 29: 1−5.

[9] WANG J L, CHEN C. Biosorbents for heavy metals removal and their future [J]. Biotechnology Advances, 2009, 27: 195−226.

[10] GUIZA S. Biosorption of heavy metal from aqueous solution using cellulosic waste orange peel [J]. Ecological Engineering, 2017, 99: 134−140.

[11] BIRUNGI Z, CHIRWA E. The kinetics of uptake and recovery of lanthanum using freshwater algae as biosorbents: Comparative analysis [J]. Bioresource Technology, 2014, 160: 43−51.

[12] PERES E C, CUNHA J M, DORTZBACHER G F, PAVAN F A, LIMA É C, FOLETTOE L, DOTTO G L. Treatment of leachates containing cobalt by adsorption on *Spirulina* sp. and activated charcoal [J]. Journal of Environmental Chemical Engineering, 2018, 6: 677−685.

[13] SAMADI-MAYBODI A, RAHMATI A. Dual metal zeolitic imidazolate frameworks as an organometallic polymer for effective adsorption of chlorpyrifos in aqueous solution [J]. Environmental Engineering Research, 2020, 25: 847−853.

[14] HU Q L, WANG L S, YU N N, ZHANG Z F, ZHENG X, HU X M. Preparation of Fe_3O_4@C@TiO_2 and its application for oxytetracycline hydrochloride adsorption [J]. Rare Metals, 2020, 39: 1333−1340.

[15] SID D, SALEM Y, BAITICHE M, DJEROUA F, BOUKHALFA N, BOUTAHALA M. Removal of methylene blue dye from water with low cost Nigella sativa seeds waste: Kinetic, isotherm, and statistical modeling [J]. Desalination and Water Treatment, 2020, 197: 358−367.

[16] SOLEIMANPOUR M, TAMADDON A M, KADIVAR M, ABOLMAALI S S, SHEKARCHIZADEH H. Fabrication of nanostructured mesoporous starch encapsulating soy-derived phytoestrogen (genistein) by well-tuned solvent exchange method [J]. International Journal of Biological Macromolecules, 220, 159: 1031−1047.

[17] CHOUDHARY B C, PAUL D, BORSE A U, GAROLE D J. Surface functionalized biomass for adsorption and recovery of gold from electronic scrap and refinery wastewater [J]. Separation and Purification Technology, 2018, 195: 260−270.

[18] LIANG Y T, HAN J W, AI C B, QIN W Q. Adsorption and leaching behaviors of chalcopyrite by two extreme thermophilic archaea [J]. Transactions of Nonferrous Metals Society of China, 2018, 28: 2538−2544.

[19] XIAO Y, FENG N N, WANG R H, DONG H G, GUO Z W, CUI H, WU H Y, LIU X X, XIE J P. Application of modified sepiolite as reusable adsorbent for Pd(II) sorption from acidic solutions [J]. Transactions of Nonferrous Metals Society of China, 2020, 30: 1375−1386.

[20] YADAV N, MADDHESHIAYA D N, RAWAT S, SINGH J. Adsorption and equilibrium studies of phenol and para-nitrophenol by magnetic activated carbon synthesised from cauliflower waste [J]. Environmental Engineering Research, 2020, 25: 742−752.

[21] DURAN C, OZDES D, GUNDOGDU A, SENTURK H B. Kinetics and isotherm analysis of basic dyes adsorption onto almond shell (prunus dulcis) as a low cost adsorbent [J]. Journal of Chemical & Engineering Data, 2011, 56: 2136−2147.

[22] NI C, CAROLAN D, ROCKS C, HUI J, FANG Z, PADMANABAN D B, NI J, XIE D, MAGUIRE P, IRVINE J T S, MARIOTTI D. Microplasma-assisted electrochemical synthesis of Co_3O_4 nanoparticles in absolute ethanol for energy applications [J]. Green Chemistry, 2018, 20: 2101−2109.

[23] GUO S M, MA L C, SONG G J, LI X R, LI P Y, WANG M Y, SHI L L, GU Z, HUANG Y D. Covalent grafting of triazine derivatives onto graphene oxide for preparation of epoxy composites with improved interfacial and mechanical properties [J]. Journal of Materials Science, 2018, 53: 16318−16330.

[24] SARMA S C, SUBBARAO U, KHULBE Y, JANA R, PETER S C. Are we underrating rare earths as an electrocatalyst? The effect of their substitution in palladium nanoparticles enhances the activity towards ethanol oxidation reaction [J]. Journal of Materials Chemistry A, 2017, 44: 23369−23381.

[25] ÇELEKLI A, YAVUZATMACA M, BOZKURT H. An eco–friendly process: Predictive modeling of copper adsorption from aqueous solution on *Spirulina platensis* [J]. Journal of Hazardous Materials, 2010, 173: 123−129.

[26] LARROSA A P Q, CAMARA Á S, MOURA J M, PINTO L A A. *Spirulina* sp. biomass dried/disrupted by different methods and their application in biofilms production [J]. Food Science and Biotechnology, 2018, 27: 1659−1665.

[27] SÖNMEZAY A, ÖNCEL M S, BEKTAŞ N. Adsorption of lead and cadmium ions from aqueous solutions using manganoxide minerals [J]. Transactions of Nonferrous Metals Society of China, 2012, 22: 3131−3139.

[28] JIANG L, ZHANG W, LUO C G, CHENG D J, ZHU J Q. Adsorption toward trivalent rare earth element from aqueous solution by zeolitic imidazolate frameworks [J]. Industrial & Engineering Chemistry Research, 2016, 55: 6365−6372.

[29] LEE Y R, YU K, RAVI S, AHN W S. Selective adsorption of rare earth elements over functionalized Cr-MIL-101 [J]. ACS Applied Materials & Interfaces, 2018, 10: 23918−23927.

[30] ELSAIDI S K, SINNWELL M A, DEVARAJ A, DROUBAY T C, NIE Z, MURUGESAN V, MCGRAIL B P, THALLAPALLY P K. Extraction of rare earth elements using magnetite@MOF composites [J]. Journal of Materials Chemistry A, 2018, 6: 18438−18443.

[31] PENG Y G, HUANG H L, ZHANG Y X, KANG C F, CHEN S M, SONG L, LIU D H, ZHONG C L. A versatile MOF-based trap for heavy metal ion capture and dispersion [J]. Nature Communications, 2018, 9: 1−9.

螺旋藻粉生物质回收稀土元素 Yb(III)：吸附等温线、动力学和热力学

舒 庆，廖春发，邹文强，许宝泉，谭育慧

江西理工大学 材料冶金化学学部，赣州 341000

摘 要：研究以螺旋藻粉作为吸附剂从废水溶液中回收 Yb(III)的吸附特性和机理。利用 SEM 和 XPS 对吸附剂的表面结构以及元素价态进行分析,探究螺旋藻粉对 Yb(III)的吸附机理；通过吸附等温线、动力学和热力学模型分析螺旋藻粉对 Yb(III)的吸附特性。Langmuir 模型表明，当温度为 318 K 时，螺旋藻粉对 Yb(III)的最大吸附量为 72.46 mg/g。动力学实验结果表明，拟二级动力学模型能较好地模拟螺旋藻粉对 Yb(III)的吸附过程，化学吸附为螺旋藻粉吸附 Yb(III)的控速步骤。吸附−脱附循环实验结果表明，螺旋藻粉具有良好的稳定性和重复使用性，是一种高效且经济的 Yb(III)回收材料。

关键词：螺旋藻粉；Yb(III)；吸附；热力学；动力学

(Edited by Xiang-qun LI)